UNIVERSITY OF WEST BOHEMIA

Applied and Computational Mechanics 1 (2007) 77 - 86

Applied and Computational Mechanics

Blade dynamic stress analysis of rotating bladed disks

J. Kellner[a,*], V. Zeman[a]

[a] *Faculty of Applied Sciences, UWB in Pilsen, Univerzitní 22, 306 14 Plzeň, Czech Republic*

Received 10 September 2007; received in revised form 24 September 2007

Abstract

The paper deals with mathematical modelling of steady forced bladed disk vibrations and with dynamic stress calculation of the blades. The blades are considered as 1D kontinuum elastic coupled with three-dimensional elastic disk centrally clamped into rotor rotating with constant angular speed. The steady forced vibrations are generated by the aerodynamic forces acting along the blade length. By using modal synthesis method the mathematical model of the rotating bladed disk is condensed to calculate steady vibrations. Dynamic stress analysis of the blades is based on calculation of the time dependent reduced stress in blade cross-sections by using Hubert-Misses-Hencky stress hypothesis. The presented method is applied to real turbomachinery rotor with blades connected on the top with shroud.
©2007 University of West Bohemia. All rights reserved.

Keywords: rotating disk, stress analysis, forced vibration

1. Introduction

The rotating systems are often modelled as one-dimensional rotating bodies with rigid disks attached to them [3], [7], [8]. Previously created model of the rotating bladed disk [9] has been applied for bladed disk forced vibration [2]. Using real disk properties and excitation by aerodynamic forces [4] there is determined dynamic behaviour of individual blades as well as of the disk. For blade dynamic stress analysis and successive high-cyclic fatigue failures there is the need to transform the forced vibration into stress response. The aim of this article is to develop an original method for stress analysis in different locations of the arbitrary blade using 3D modelling of the disk [5], 1D modelling of the blades [1] and reduction of number of bladed disk DOF by modal synthesis method.

2. Mathematical model of the rotating bladed disk

The rotating bladed disk can be generally decomposed into disk (subsystem D) and separated blade packets (subsystems $P_s,\ s = 1, 2, \ldots, p$), where p is their count (fig. 1). We assume that the disk is centrally clamped into turbomachine rotor rotating with constant angular speed ω. The disk nodes on the inner radius are fixed in all directions. The blades (B_j) in packets (P_s) are connected on the top with shrouds (S). The blades elastic seating to disk is replaced with elastic supports in outer contact points of two dog bolts between disk and every one blade foot. The blade packets are mutually connected by elastic linkages characterized by diagonal stiffness matrix $\boldsymbol{K}_L = diag(k_u,\ k_v,\ k_w,\ k_\varphi,\ k_\vartheta,\ k_\psi)$.

*Corresponding author. Tel.: +420 377 632 384, e-mail: josef.kellner@zcu.cz.

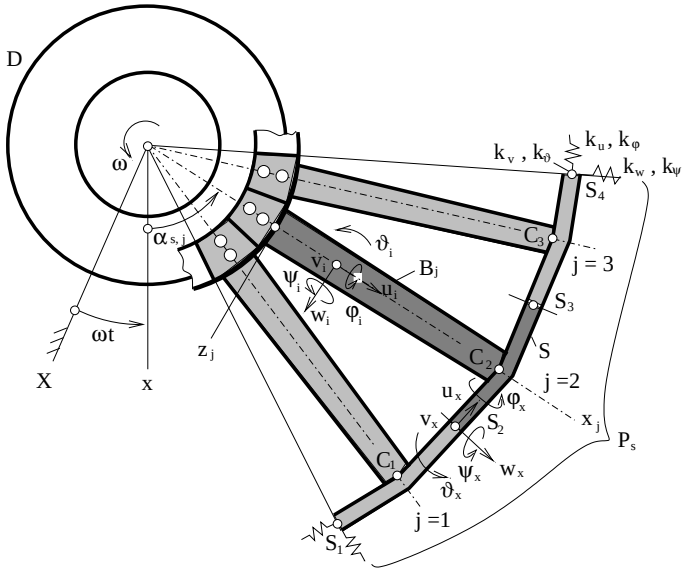

Fig. 1. Scheme of the bladed disk with detail of one blade packet.

The mathematical model of the undamped subsystems incorporated in the rotating bladed disk can be written in matrix form [5], [9]

$$\boldsymbol{M}_D\ddot{\boldsymbol{q}}_D(t) + \omega\boldsymbol{G}_D\dot{\boldsymbol{q}}_D(t) + \left(\boldsymbol{K}_{\mathbf{s}D} - \omega^2\boldsymbol{K}_{dD}\right)\boldsymbol{q}_D(t) = \omega^2\boldsymbol{f}_D + \boldsymbol{f}_D^C\,, \tag{1}$$

$$\boldsymbol{M}_P\ddot{\boldsymbol{q}}_{P,s}(t) + \omega\boldsymbol{G}_P\dot{\boldsymbol{q}}_{P,s}(t) + \left(\boldsymbol{K}_{\mathbf{s}P} - \omega^2\boldsymbol{K}_{dP} + \omega^2\boldsymbol{K}_{\omega P}\right)\boldsymbol{q}_{P,s}(t) = \omega^2\boldsymbol{f}_P + \boldsymbol{f}_{P,s}^C + \boldsymbol{f}_{P,s}(t), \tag{2}$$

$s = 1, 2, \ldots, p$, where mass matrices $\boldsymbol{M}_D$, $\boldsymbol{M}_P$, static stiffness matrices $\boldsymbol{K}_{\mathbf{s}D}, \boldsymbol{K}_{\mathbf{s}P}$ and dynamic stiffness matrices $\boldsymbol{K}_{dD}$, $\boldsymbol{K}_{dP}$ of the disk (subscript D) and blade packets (subscript P) are symmetrical. Symmetric matrix $\boldsymbol{K}_{\omega P}$ expresses a centrifugal blade stiffening [1]. Skew-symmetric matrices $\omega\boldsymbol{G}_D$ and $\omega\boldsymbol{G}_P$ express gyroscopic effects. Centrifugal load vectors $\omega^2\boldsymbol{f}_D$ and $\omega^2\boldsymbol{f}_P$ are constant in time. Vectors $\boldsymbol{f}_{P,s}(t)$ express the excitation of the blade packets by aerodynamic forces. All presented matrices in models (1) and (2) correspond to mutually uncoupled subsystems and are created by means of finite element method (for more details see contributions [1], [9], [5]). Vectors $\boldsymbol{f}_D^C$ and $\boldsymbol{f}_{P,s}^C$ ($s = 1, 2, \ldots, p$) represent the coupling forces in general coordinates of subsystems

$$\boldsymbol{q}_D = \left[\ldots\ u_i^{(D)}\ v_i^{(D)}\ w_i^{(D)}\ \ldots\right]^T \in \mathcal{R}^{n_D}, \tag{3}$$

$$\boldsymbol{q}_{P,s} = \left[\boldsymbol{q}_{S_1}^T\boldsymbol{q}_{B,1}^T\boldsymbol{q}_{S_2}^T\boldsymbol{q}_{B,2}^T\boldsymbol{q}_{S_3}^T\boldsymbol{q}_{B,3}^T\boldsymbol{q}_{S_4}^T\right]_{P,s}^T \in \mathcal{R}^{n_P}, \tag{4}$$

where $u_i^{(D)}$, $v_i^{(D)}$, $w_i^{(D)}$ in (3) are disk nodal displacements in direction of disk rotating axis x, y, z (fig. 2). Coordinates of subvectors $\boldsymbol{q}_{B,j}$ ($j = 1, 2, 3$) express the blade displacements of the node i (fig. 1) in direction of rotating axis x_j, y_j, z_j and small turn angles of the blade cross section (subscript j corresponds to blade in packet)

$$\boldsymbol{q}_{B,j} = [\ldots\ u_i\ v_i\ w_i\ \varphi_i\ \vartheta_i\ \psi_i\ \ldots]_{B,j}^T\ , \quad i = 1, 2, \ldots, N, \quad j = 1, 2, 3. \tag{5}$$

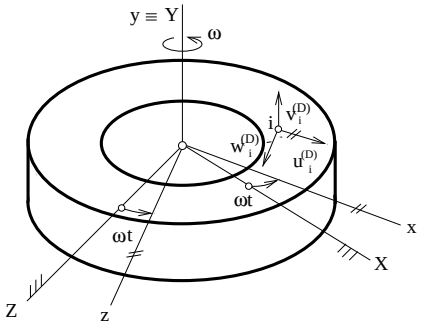

Fig. 2. Scheme of the disk.

Coordinates of subvectors $\boldsymbol{q}_{S_1}$,$\boldsymbol{q}_{S_2,\ldots}$ express the shroud's displacements in nodes $S_1,\ S_2, \ldots$

$$\boldsymbol{q}_x = [u_x\ v_x\ w_x\ \varphi_x\ \vartheta_x\ \psi_x]^T_{P,s}\ , \quad x = S_1,\ S_2, \ldots \tag{6}$$

Vector $\boldsymbol{f}^C_D$ represents the forces in all blade's seating to disk acting on the disk. Vector $\boldsymbol{f}^C_{P,s}$ expresses the coupling forces in blade's seating of packet s and in shroud linkages between blade packets acting on single packet s.

The global coupling force vector in global configuration space of all general coordinates

$$\boldsymbol{q} = \left[\boldsymbol{q}^T_D\ \boldsymbol{q}_{P,1}\ \boldsymbol{q}_{P,2}\ \ldots \boldsymbol{q}_{P,p}\right]^T \tag{7}$$

can be calculated from the potential (strain) energy as

$$\boldsymbol{f}_C = \begin{bmatrix} \boldsymbol{f}^C_D \\ \boldsymbol{f}^C_{P,1} \\ \vdots \\ \boldsymbol{f}^C_{P,p} \end{bmatrix} = -\frac{\partial E^C_p}{\partial \boldsymbol{q}}\,. \tag{8}$$

This energy can be expressed in the additive form

$$E^C_p = \sum_{s=1}^{p}\sum_{j=1}^{b} E^C_{s,j} + E^C_P\,, \tag{9}$$

where $E^C_{s,j}$ is coupling strain energy between blade j in blade packet s and the disk and the E^C_P is strain energy of all shroud linkages between blade packets. The linearized global coupling force vector can be written in the form

$$\boldsymbol{f}_C = -\sum_{s=1}^{p}\sum_{j=1}^{b} \boldsymbol{K}^C_{s,j}\boldsymbol{q} - \boldsymbol{K}^C_P\boldsymbol{q}\,. \tag{10}$$

The coupling stiffness matrices result from equations conform the conditions

$$\frac{\partial E^C_{s,j}}{\partial \boldsymbol{q}} = \boldsymbol{K}^C_{s,j}\boldsymbol{q}\,, \quad \frac{\partial E^C_P}{\partial \boldsymbol{q}} = \boldsymbol{K}^C_P\boldsymbol{q}\,. \tag{11}$$

The mathematical models (1), (2) using (8) and (10) after completion of a damping in couplings can be rewritten in the global matrix form

$$\begin{bmatrix} \boldsymbol{M}_D & \boldsymbol{0} \\ \boldsymbol{0} & \boldsymbol{M}_R \end{bmatrix} \begin{bmatrix} \ddot{\boldsymbol{q}}_D(t) \\ \ddot{\boldsymbol{q}}_R(t) \end{bmatrix} + \left(\boldsymbol{B}^C_P + \sum_{s=1}^{p}\sum_{j=1}^{b} \boldsymbol{B}^C_{s,j} + \omega \begin{bmatrix} \boldsymbol{G}_D & \boldsymbol{0} \\ \boldsymbol{0} & \boldsymbol{G}_R \end{bmatrix} \right) \begin{bmatrix} \dot{\boldsymbol{q}}_D(t) \\ \dot{\boldsymbol{q}}_R(t) \end{bmatrix} +$$

$$+ \left(\begin{bmatrix} \boldsymbol{K}_D(\omega) & \boldsymbol{0} \\ \boldsymbol{0} & \boldsymbol{K}_R(\omega) \end{bmatrix} + \sum_{s=1}^{p}\sum_{j=1}^{b} \boldsymbol{K}^C_{s,j} \right) \begin{bmatrix} \boldsymbol{q}_D(t) \\ \boldsymbol{q}_R(t) \end{bmatrix} = \omega^2 \begin{bmatrix} \boldsymbol{f}_D \\ \boldsymbol{f}_C \end{bmatrix} + \begin{bmatrix} \boldsymbol{0} \\ \boldsymbol{f}_R(t) \end{bmatrix}, \tag{12}$$

where

$$\boldsymbol{q}_R \;=\; \left[\boldsymbol{q}_{P,1}^T \quad \boldsymbol{q}_{P,2}^T \;\ldots\; \boldsymbol{q}_{P,p}^T\right]^T \in \mathcal{R}^{n_R}\,,\; n_R = p\,n_P \tag{13}$$

is the general coordinate vector of a blading with shroud creating the blade rim (subscript R). The global stiffness matrix of the rotating disk has the form

$$\boldsymbol{K}_D(\omega) \;=\; \boldsymbol{K}_{\mathbf{s}D} - \omega^2 \boldsymbol{K}_{dD} \;\in \mathcal{R}^{n_D,n_D}\,. \tag{14}$$

The matrices of the blade rim are compiled from the blade packet matrices

$$\boldsymbol{X}_R \;=\; diag\,(\boldsymbol{X}_P,\, \boldsymbol{X}_P, \ldots \boldsymbol{X}_P,\,) \in \mathcal{R}^{n_R,n_R}\,,\; \boldsymbol{X} \;=\; \boldsymbol{M}, \boldsymbol{G}, \boldsymbol{K}_{\mathbf{s}}, \boldsymbol{K}_d, \boldsymbol{K}_\omega. \tag{15}$$

The global stiffness blade rim matrix is

$$\boldsymbol{K}_R(\omega) \;=\; \boldsymbol{K}_{\mathbf{s}R} + \omega^2\left(\boldsymbol{K}_{\omega R} - \boldsymbol{K}_{dR}\right) + \boldsymbol{K}_{PP}^C \;\in \mathcal{R}^{n_R,n_R}\,, \tag{16}$$

where $\boldsymbol{K}_{PP}^C$ is nonzero submatrix of the coupling stiffness matrix $\boldsymbol{K}_P^C$ corresponding to subsystem R.

The centrifugal load vector of the blade rim is

$$\boldsymbol{f}_C \;=\; \left[\boldsymbol{f}_P^T\; \boldsymbol{f}_P^T \;\ldots\; \boldsymbol{f}_P^T\right]^T \in \mathcal{R}^{n_R} \tag{17}$$

and vector of the aerodynamic forces has the general form

$$\boldsymbol{f}_R(t) \;=\; \left[\boldsymbol{f}_{P,1}^T(t),\, \boldsymbol{f}_{P,2}^T(t),\, \ldots\,,\, \boldsymbol{f}_{P,p}^T(t)\right]^T \in \mathcal{R}^{n_R}\,. \tag{18}$$

It is advantageous to assemble condensed mathematical model of the rotating bladed disk with reduced degrees of freedom (DOF) number, because mainly the three-dimensional elastic disk could have large DOF number n_D and blade rim DOF number is $n_R = p\,n_P$.

The modal transformations

$$\boldsymbol{q}_D(t) \;=\; {}^m\boldsymbol{V}_D \boldsymbol{x}_D(t)\,, \quad \boldsymbol{q}_R(t) \;=\; {}^m\boldsymbol{V}_R \boldsymbol{x}_R(t) \tag{19}$$

are introduced for this purpose. Matrices ${}^m\boldsymbol{V}_D \in \mathcal{R}^{n_D,m_D}$ and ${}^m\boldsymbol{V}_R \in \mathcal{R}^{n_R,m_R}$ are "master" modal submatrices of subsystems D (disk) and R (blade rim) obtained from modal analysis of the mutually uncoupled ($\boldsymbol{K}_{s,j}^C = \boldsymbol{0}$ for all $s,\, j$) and non-rotating subsystems represented by models

$$\boldsymbol{M}_D \ddot{\boldsymbol{q}}_D(t) + \boldsymbol{K}_{\mathbf{s}D}\boldsymbol{q}_D(t) = \boldsymbol{0}\,, \quad \boldsymbol{M}_R \ddot{\boldsymbol{q}}_R(t) + \left(\boldsymbol{K}_{\mathbf{s}R} + \boldsymbol{K}_{PP}^C\right)\boldsymbol{q}_R(t) = \boldsymbol{0}\,. \tag{20}$$

A condensation (reduction in DOF number) of both systems is attached by selection of a set of m_D and m_R subsystem master mode shapes ($m_D < n_D$, $m_R < n_R$). The new configuration space of dimension $m = m_D + m_R$ is defined by coordinate vector

$$\boldsymbol{x}(t) \;=\; \left[\boldsymbol{x}_D^T(t) \quad \boldsymbol{x}_R^T(t)\right]^T \in \mathcal{R}^m\,. \tag{21}$$

After the transformations (19) with considerations of the orthonormality conditions ${}^m\boldsymbol{V}_D^T \boldsymbol{M}_D\, {}^m\boldsymbol{V}_D \;=\; \boldsymbol{E}_D$ and ${}^m\boldsymbol{V}_R^T \boldsymbol{M}_R\, {}^m\boldsymbol{V}_R \;=\; \boldsymbol{E}_R$ the model (12) can be rewritten in the condensed form

$$\begin{aligned} &\ddot{\boldsymbol{x}}(t) + \left(\tilde{\boldsymbol{B}} + \omega\tilde{\boldsymbol{G}}\right)\dot{\boldsymbol{x}}(t) + \\ &+ \left(\boldsymbol{\Lambda} + \omega^2\left(\tilde{\boldsymbol{K}}_\omega - \tilde{\boldsymbol{K}}_d\right) + \boldsymbol{V}^T\left(\sum_{s=1}^{p}\sum_{j=1}^{b}\boldsymbol{K}_{s,j}^C\right)\boldsymbol{V}\right)\boldsymbol{x}(t) \;= \boldsymbol{V}^T\left(\omega^2\boldsymbol{f}_0 + \boldsymbol{f}(t)\right)\,, \end{aligned} \tag{22}$$

where

$$\tilde{\boldsymbol{B}} = \boldsymbol{V}^T \left(\boldsymbol{B}_P^C + \sum_{s=1}^{p} \sum_{j=1}^{b} \boldsymbol{B}_{s,j}^C \right) \boldsymbol{V},$$

$$\tilde{\boldsymbol{X}} = diag \left({}^m\boldsymbol{V}_D^T \boldsymbol{X}_D \, {}^m\boldsymbol{V}_D \,, \quad {}^m\boldsymbol{V}_R^T \boldsymbol{X}_R \, {}^m\boldsymbol{V}_R \right) \in \mathcal{R}^{m,m}$$

for $\boldsymbol{X} = \boldsymbol{G}$, $\boldsymbol{K}_d$, $\boldsymbol{K}_\omega$ (with $\boldsymbol{K}_{\omega D} = \boldsymbol{0}$). Matrices

$$\boldsymbol{\Lambda} = diag \left({}^m\boldsymbol{\Lambda}_D \,, \quad {}^m\boldsymbol{\Lambda}_R \right) \,, \quad \boldsymbol{V} = diag \left({}^m\boldsymbol{V}_D \,, \, {}^m\boldsymbol{V}_R \right) \tag{23}$$

are composed from spectral and modal submatrices of the subsystems satisfying the conditions

$${}^m\boldsymbol{V}_D^T \boldsymbol{K}_{\mathbf{s}D} \, {}^m\boldsymbol{V}_D = {}^m\boldsymbol{\Lambda}_D \,, \quad {}^m\boldsymbol{V}_R^T \left(\boldsymbol{K}_{\mathbf{s}R} + \boldsymbol{K}_{PP}^C \right)^m \boldsymbol{V}_R = {}^m\boldsymbol{\Lambda}_R \,. \tag{24}$$

The vector $\boldsymbol{f}_0 = \left[\boldsymbol{f}_D^T \,, \, \boldsymbol{f}_C^T \right]^T$ expresses the influence of the centrifugal forces. The global vector of the aerodynamic forces in complex form is $\boldsymbol{f}(t) = \boldsymbol{f} e^{i\omega_k t}$, where $\boldsymbol{f} = \left[\boldsymbol{0}^T \; \boldsymbol{f}_R^T \right]^T$. We assume the harmonic blade excitation in axial (outspread to turbomachine rotor) and circumferential (tangential) direction concentrated in blade nodes i (fig. 1) in the complex form

$$\boldsymbol{f}_{B,j}(t) = [\ldots; F_{iy} \cos \varphi_{j,s} + i F_{iy} \sin \varphi_{j,s}; F_{iz} \cos \psi_{j,s} + i F_{iz} \sin \psi_{j,s}; \ldots] \, e^{i\omega_k t} \,, \tag{25}$$

where ω_k is dominant excitation frequency corresponding to number of stator nozzles multiply angular velocity of the rotating disk. The angle $\varphi_{j,s}$ is the phase angle of the aerodynamic forces acting on j-th blade in s-th blade packet in the axial direction and $\psi_{j,s}$ is the phase angle in tangential direction on the same blade. These phase angles can be expressed in the form

$$\varphi_{j,s} = [j - 1 + (s-1)3] \, 2\pi \frac{p_{SB}}{p_{MB}} \,, \qquad \psi_{j,s} = \varphi_{j,s} - \varphi \,, \tag{26}$$

where φ is the relative phase shift between aerodynamic forces applied in axial and circumferential direction [4] and p_{SB} (p_{MB}) is stator (rotor) blade number.

3. Forced vibration and stress analysis

For high-cycle fatigue we consider only aerodynamic forces acting on the moving blades, that's why we don't use below the constant centrifugal force $\boldsymbol{f}_0$ presented in (22). The steady dynamic response of the rotating bladed disk calculated at the condensed model (22) is of the form $\boldsymbol{x}(t) = \boldsymbol{x} e^{i\omega_k t}$ with complex amplitude vector

$$\boldsymbol{x} = \boldsymbol{Z}^{-1} \boldsymbol{V}^T \boldsymbol{f} \,, \tag{27}$$

where

$$\boldsymbol{Z} = -\omega_k^2 \boldsymbol{E} + i\omega_k \left(\tilde{\boldsymbol{B}} + \omega \tilde{\boldsymbol{G}} \right) + \left(\boldsymbol{\Lambda} + \omega^2 \left(\tilde{\boldsymbol{K}}_\omega - \tilde{\boldsymbol{K}}_d \right) + \boldsymbol{V}^T \left(\sum_{s=1}^{p} \sum_{j=1}^{b} \boldsymbol{K}_{s,j}^C \right) \boldsymbol{V} \right) \tag{28}$$

is the dynamic stiffness matrix of the condensed model and $\boldsymbol{f}$ is vector of the complex amplitudes of the aerodynamic excitation. Damping matrices $\boldsymbol{B}_P^C$ and $\boldsymbol{B}_{s,j}^C$ are considered as proportional to stiffness matrices of the corresponding couplings. By using modal transformation we obtain the steady state solution in global configuration space

$$\boldsymbol{q} e^{i\omega_k t} = \boldsymbol{V} \boldsymbol{x} e^{i\omega_k t} \,. \tag{29}$$

This solution has the complex form and the real displacements of the excited rotating bladed disk is the real part of the complex generalized coordinate vector

$$\boldsymbol{q}(t) \;=\; Re\{\boldsymbol{q}e^{i\omega_k t}\}\,. \tag{30}$$

Stress intensity in any point on the blade profil in distance ξ from beginning of actual blade element e (see fig. 3) and determined by coordinates $\eta,\ \zeta$ from gravity center of profile is expressed by stress vector

$$\boldsymbol{\sigma}^{(e)}(\xi,\,\eta,\,\zeta,\,t) = \left[\sigma_\xi^{(e)}\,\sigma_\eta^{(e)}\,\sigma_\zeta^{(e)}\,\tau_{\eta\zeta}^{(e)}\,\tau_{\zeta\xi}^{(e)}\,\tau_{\xi\eta}^{(e)}\right]^T\,. \tag{31}$$

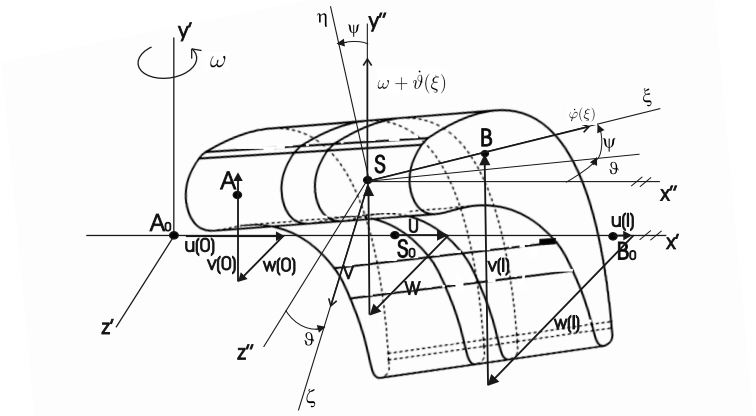

Fig. 3. Scheme of blade element.

Using extension $\boldsymbol{\varepsilon}$ it can be expressed in form

$$\boldsymbol{\sigma}^{(e)}(\xi,\,\eta,\,\zeta,\,t) = \boldsymbol{D}\boldsymbol{\varepsilon}^{(e)}\,(\xi,\eta,\zeta,t)\;, \tag{32}$$

where

$$\boldsymbol{D} \;=\; \frac{E}{(1+\nu)(1-2\nu)}\begin{bmatrix} 1-\nu & \nu & \nu & 0 & 0 & 0 \\ \nu & 1-\nu & \nu & 0 & 0 & 0 \\ \nu & \nu & 1-\nu & 0 & 0 & 0 \\ 0 & 0 & 0 & \frac{1}{2}(1-2\nu) & 0 & 0 \\ 0 & 0 & 0 & 0 & \frac{1}{2}(1-2\nu) & 0 \\ 0 & 0 & 0 & 0 & 0 & \frac{1}{2}(1-2\nu) \end{bmatrix} \tag{33}$$

and $\boldsymbol{\varepsilon}^{(e)} \;=\; \left[\varepsilon_\xi^{(e)}\,\varepsilon_\eta^{(e)}\,\varepsilon_\zeta^{(e)}\,\gamma_{\eta\zeta}^{(e)}\,\gamma_{\zeta\xi}^{(e)}\,\gamma_{\xi\eta}^{(e)}\right]^T$. From Cauchy geometrical equations [6] we can obtain the forms for components of the strain vector $\boldsymbol{\varepsilon}^{(e)}$ (superscript (e) is hereafter let out):

$$\begin{array}{lll} \varepsilon_\xi \;=\; \frac{\partial u_\xi}{\partial \xi}, & \varepsilon_\eta \;=\; \frac{\partial u_\eta}{\partial \eta}, & \varepsilon_\zeta \;=\; \frac{\partial u_\zeta}{\partial \zeta}, \\ \gamma_{\xi\eta} \;=\; \frac{\partial u_\xi}{\partial \eta} + \frac{\partial u_\eta}{\partial \xi}, & \gamma_{\eta\zeta} \;=\; \frac{\partial u_\eta}{\partial \zeta} + \frac{\partial u_\zeta}{\partial \eta}, & \gamma_{\zeta\xi} \;=\; \frac{\partial u_\zeta}{\partial \xi} + \frac{\partial u_\xi}{\partial \zeta}, \end{array} \tag{34}$$

where due to [1] is known that

$$u_\xi \;=\; u - \eta\psi + \zeta\vartheta,\; u_\eta \;=\; v - \zeta\varphi,\; u_\zeta \;=\; w + \eta\varphi,\; \psi \;=\; v',\; \vartheta \;=\; -w' \tag{35}$$

which leads to expressions

$$\begin{aligned}
\varepsilon_\xi &= u'(\xi) - \eta v''(\xi) - \zeta w''(\xi) = \boldsymbol{\Psi}' \boldsymbol{S}_3^{-1} \boldsymbol{q}_3 - \eta \boldsymbol{\Phi}'' \boldsymbol{S}_1^{-1} \boldsymbol{q}_1 - \zeta \boldsymbol{\Phi}'' \boldsymbol{S}_2^{-1} \boldsymbol{q}_2, \\
\varepsilon_\eta &= v'(\xi) - \zeta \varphi'(\xi) = \boldsymbol{\Phi}' \boldsymbol{S}_1^{-1} \boldsymbol{q}_1 - \zeta \boldsymbol{\Psi}' \boldsymbol{S}_3^{-1} \boldsymbol{q}_4, \\
\varepsilon_\zeta &= w'(\xi) + \eta \varphi'(\xi) = \boldsymbol{\Phi}' \boldsymbol{S}_2^{-1} \boldsymbol{q}_2 + \eta \boldsymbol{\Psi}' \boldsymbol{S}_3^{-1} \boldsymbol{q}_4, \\
\gamma_{\xi\eta} &= -v'(\xi) + v'(\xi) - \zeta \varphi'(\xi) = -\zeta \boldsymbol{\Psi}' \boldsymbol{S}_3^{-1} \boldsymbol{q}_4, \\
\gamma_{\eta\zeta} &= -\varphi(\xi) + \varphi(\xi) = 0, \\
\gamma_{\zeta\xi} &= w' + \eta \varphi'(\xi) - w' = \eta \boldsymbol{\Psi}' \boldsymbol{S}_3^{-1} \boldsymbol{q}_4.
\end{aligned} \tag{36}$$

The displacements of internal points of the blade element were approximated by neglecting shear deformations in the form

$$\begin{aligned}
u(\xi) = \boldsymbol{\Phi} \boldsymbol{S}_3^{-1} \boldsymbol{q}_3, \quad v(\xi) = \boldsymbol{\Phi} \boldsymbol{S}_1^{-1} \boldsymbol{q}_1, \quad w(\xi) = \boldsymbol{\Phi} \boldsymbol{S}_2^{-1} \boldsymbol{q}_2, \\
\varphi(\xi) = \boldsymbol{\Psi} \boldsymbol{S}_3^{-1} \boldsymbol{q}_4, \quad \vartheta(\xi) = -\boldsymbol{\Phi}' \boldsymbol{S}_2^{-1} \boldsymbol{q}_2, \quad \psi(\xi) = \boldsymbol{\Phi}' \boldsymbol{S}_1^{-1} \boldsymbol{q}_1,
\end{aligned} \tag{37}$$

where $\boldsymbol{\Phi} = [1\ \xi\ \xi^2\ \xi^3]$, $\boldsymbol{\Psi} = [1\ \xi]$ and vector of node displacements of the blade elements of length $\mathrm{A}_0\,\mathrm{B}_0 = l$ was decomponated to subvectors

$$\begin{aligned}
\boldsymbol{q}_1 = [v(0)\ \psi(0)\ v(l)\ \psi(l)]^T, \qquad \boldsymbol{q}_2 = [w(0)\ \vartheta(0)\ w(l)\ \vartheta(l)]^T, \\
\boldsymbol{q}_3 = [u(0)\ u(l)]^T, \qquad \boldsymbol{q}_4 = [\varphi(0)\ \varphi(l)]^T.
\end{aligned} \tag{38}$$

The form of matrices $\boldsymbol{S}_i,\ i = 1, 2, 3$ is presented in [1].

Using relations (36) the strain vector can be rewritten into the matrix form

$$\boldsymbol{\varepsilon}^{(e)}(\xi, \eta, \zeta, t) = \boldsymbol{A}^{(e)}(\xi, \eta, \zeta) \boldsymbol{q}^{(e)}(t)$$

$$\begin{bmatrix} \varepsilon_\xi \\ \varepsilon_\eta \\ \varepsilon_\zeta \\ \gamma_{\eta\zeta} \\ \gamma_{\zeta\xi} \\ \gamma_{\xi\eta} \end{bmatrix} = \begin{bmatrix} -\eta \boldsymbol{\Phi}'' \boldsymbol{S}_1^{-1} & -\zeta \boldsymbol{\Phi}'' \boldsymbol{S}_2^{-1} & \boldsymbol{\Psi}' \boldsymbol{S}_3^{-1} & \boldsymbol{0} \\ \boldsymbol{\Phi}' \boldsymbol{S}_1^{-1} & \boldsymbol{0} & \boldsymbol{0} & -\zeta \boldsymbol{\Psi}' \boldsymbol{S}_3^{-1} \\ \boldsymbol{0} & \boldsymbol{\Phi}' \boldsymbol{S}_2^{-1} & \boldsymbol{0} & \eta \boldsymbol{\Psi}' \boldsymbol{S}_3^{-1} \\ \boldsymbol{0} & \boldsymbol{0} & \boldsymbol{0} & \boldsymbol{0} \\ \boldsymbol{0} & \boldsymbol{0} & \boldsymbol{0} & \eta \boldsymbol{\Psi}' \boldsymbol{S}_3^{-1} \\ \boldsymbol{0} & \boldsymbol{0} & \boldsymbol{0} & -\zeta \boldsymbol{\Psi}' \boldsymbol{S}_3^{-1} \end{bmatrix} \begin{bmatrix} \boldsymbol{q}_1 \\ \boldsymbol{q}_2 \\ \boldsymbol{q}_3 \\ \boldsymbol{q}_4 \end{bmatrix}. \tag{39}$$

The equation (32) applied for concrete blade element in the complex form is

$$\boldsymbol{\sigma}_{s,j}^{(e)}(\xi, \eta, \zeta) e^{i\omega_k t} = \boldsymbol{D} \boldsymbol{A}^{(e)}(\xi, \eta, \zeta) \boldsymbol{T} \tilde{\boldsymbol{q}}_{s,j}^{(e)} e^{i\omega_k t}, \tag{40}$$

where s is index of packet and j index of blade in packet s, $\boldsymbol{T}$ is transformation matrix between global and local coordinate system [1], $\tilde{\boldsymbol{q}}_{s,j}^{(e)}$ is vector of complex displacement amplitudes of the blade element in global system. That's why the real stress vector is

$$\boldsymbol{\sigma}_{s,j}^{(e)}(\xi,\, \eta,\, \zeta,\, t) = Re\left\{ \boldsymbol{\sigma}_{s,j}^{(e)}(\xi,\, \eta,\, \zeta) e^{i\omega_k t} \right\} = Re\left\{ \left(\bar{\boldsymbol{\sigma}}_{s,j}^{(e)} + i\, \bar{\bar{\boldsymbol{\sigma}}}_{s,j}^{(e)} \right) (\cos \omega_k t \,+\, i \sin \omega_k t) \right\}, \tag{41}$$

$$\boldsymbol{\sigma}_{s,j}^{(e)}(\xi,\, \eta,\, \zeta,\, t) = \bar{\boldsymbol{\sigma}}_{s,j}^{(e)} \cos \omega_k t - \bar{\bar{\boldsymbol{\sigma}}}_{s,j}^{(e)} \sin \omega_k t, \tag{42}$$

where quantities marked by bar ($\bar{x}$) are real parts and quantities with two bars ($\bar{\bar{x}}$) are imaginary parts of complex vector components. Using Hubert-Misses-Hencky stress hypothesis [6] we obtain reduced stress

$$\sigma_{red}^{(e)}(\xi,\, \eta,\, \zeta,\, t) = \frac{1}{\sqrt{2}} \sqrt{(\sigma_\xi - \sigma_\eta)^2 + (\sigma_\eta - \sigma_\zeta)^2 + (\sigma_\xi - \sigma_\zeta)^2 + 6(\tau_{\zeta\eta}^2 + \tau_{\xi\eta}^2 + \tau_{\xi\zeta}^2)}, \tag{43}$$

where $\sigma_\xi = \bar{\sigma}_\xi \cos \omega_k t - \bar{\bar{\sigma}}_\xi \sin \omega_k t$, etc.

4. Application

On the basis of the presented method the original software in MATLAB code was created. The matrices of the disk were obtained by three-dimensional finite element method as is shown in [5]. The matrices of the blade rim were derived by one-dimensional finite element method applied to blades with shroud [9]. The aerodynamic forces applied in axial and tangential direction on each moving blade were assumed from [4]. The software and the proposed approach was applied to the centrally clamped steel bladed disk characterized by following basic parameters:

disk inner/outer radius	$0.335/05754\ m$
disk thickness	$0.155\ m$
length of blades	$0.253\ m$
width/thickness of shroud with rectangular profil	$0.1005/0.014\ m$
number of blades in packets b	3
number of blade packets p	18
DOF number of the discretized disk n_D	3240
DOF number of the discretized blade ring n_R	3672
Young's modulus of the disk, blade and shroud materials E	$2e^{11}\ Pa$
Poisson's ratio ν	0.3
mass density ϱ	$7800\ kg.m^{-3}$
amplitude of global axial force F_y acting on one blade	$700\ N$
amplitude of global tangential force F_z acting on one blade	$1600\ N$
relative phase shift between F_y and F_z	25

translation stiffnesses of the flexible blade seating in disk (fig.1)

$$k_{x_j} = k_{z_j} = 2,8.10^9;\ k_{y_j} = 4,88.10^9\ Nm^{-1}$$

torsional/flexural stiffnesses of the flexible blade seating in disk (fig.1)

$$k_{x_jx_j} = 1,05.10^8;\ k_{y_jy_j} = 1,5.10^7\ \ k_{z_jz_j} = 3.10^7\ Nm.rad^{-1}$$

stiffnesses linkages between blade packets (fig.1)

$k_u = k_v = k_w = 10^9\ Nm^{-1};\ k_\varphi = k_\psi = 10^7;\ k_\vartheta = 10^6\ Nm.rad^{-1}$

The time dependent normal stress σ_ζ for excitation frequency corresponding to 3000 revolutions per minute of the disk and 32 number of stator nozzles in the blade cross-section of the third element (the location of the blade profile for $s = j,\ j = 1$ in distance $\xi = 0$ and in gravity center) is drawn in fig. 4 because it has the greatest value of stress vector components. Also there is possibility to display components of vector $\boldsymbol{\sigma}_{s,j}^{(e)}$ on the whole chosen blade profile for arbitrary instant of time. For illustration the normal stress σ_ζ (resp. σ_η) on the concrete chosen profile in time $t = 0.4\,ms$ is shown in fig. 5 (resp. fig. 6).This cross-section stress can be drawn as a movie dependent upon time. The shear stress are low order that's why they are not here presented.

5. Conclusion

The stress analysis of blades on rotating bladed disk excited by aerodynamic forces was introduced. Compare to stress conditions of High-Smith diagram it can be said that the analysed blade satisfies criterion for turbine blades in meaning of high-cycle fatigue. Presented results are obtained from model which has a cyclic symmetric structure. The introduced method and developed software will make possible to dynamic stress modelling of imperfect bladed disk caused

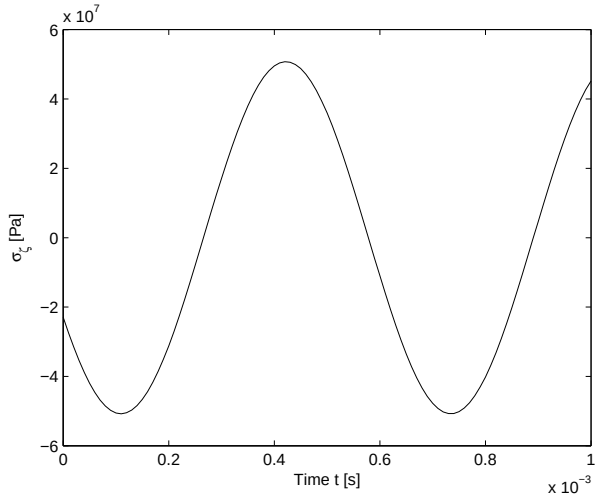

Fig. 4. Time dependent normal stress $\sigma_\zeta(0,0,0,t)$ on the third blade element $s=1,\ j=1$.

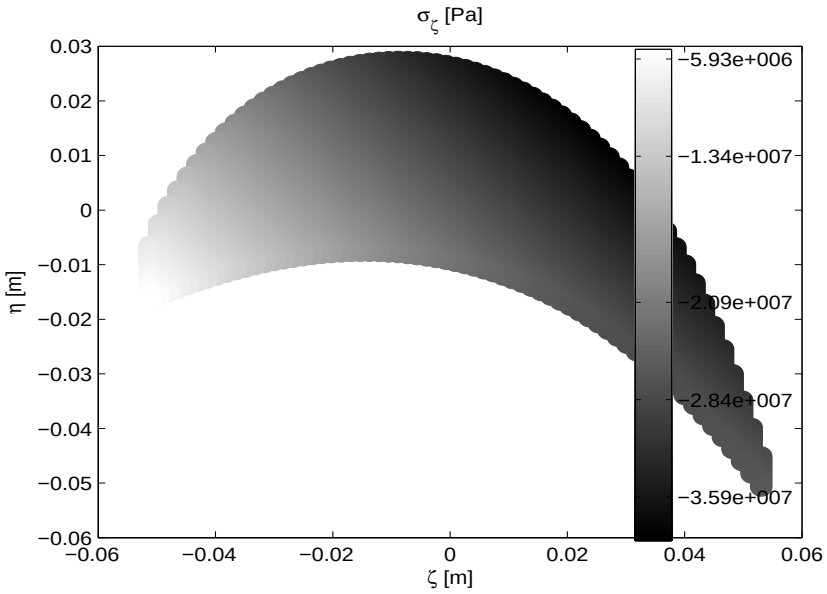

Fig. 5. Normal stress $\sigma_\zeta(0,\eta,\zeta,4e-4)$ on the third blade element $s=1,\ j=1$.

by manufacture inaccuracy. Mathematical model of rotating bladed disk in parametric form will be put to use for parameter correction on the basis of experimental data and for subsequent optimization in term of dynamic stress.

Acknowledgements

This work was supported by the research project MSM 4977751303 and the Fund for University Development FRVS 23/2007.

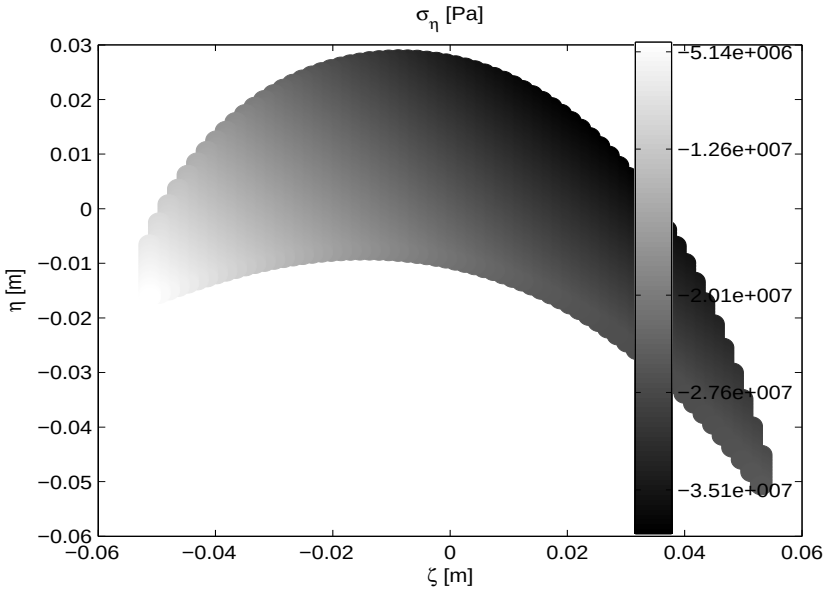

Fig. 6. Normal stress $\sigma_\eta(0, \eta, \zeta, 4e-4)$ on the third blade element $s = 1,\ j = 1$.

References

[1] J. Kellner, V. Zeman, Influence of dynamic stiffness, centrifugal forces and blade's elastic seating on blade modal properties, Proceedings of the 8th Applied Mechanics, University of West Bohemia in Pilsen, Srni, 2006, pp. 47-48 (full text on CD-ROM).

[2] J. Kellner, J. Šašek, V. Zeman, Forced vibration of the bladed disk, Proceedings of the Engineering Mechanics 2007, Svratka, 2007, pp. 113-114.

[3] E. Krămer, Dynamics of rotors and foundations, Springer-Verlag, Berlin, 1993.

[4] T. Misek, A. Tetiva, L. Prchlik, K. Duchek, Prediction of high cycle fatigue life of steam turbine blading based on unsteady CFD and FEM forced response calculation, Proceedings of the ASME Turbo Expo 2007, Montreal, 2007.

[5] J. Šašek, V. Zeman, M. Hajžman, Modal properties of the rotating disks, Proceedings of the 22nd Computional Mechanics, Nectiny, University of the West Bohemia in Pilsen, 2006, pp. 593-600.

[6] F. Trebuňa, V. Jurica, F. Šimčák, Pružnosť a pevnosť II., Vienala, Košica 2000.

[7] T. Yamamoto, Y. Ishida, Linear and nonlinear rotordynamics, a modern treatment with applications, John Wiley & Sons, New York, 2001.

[8] V. Zeman, Z. Hlav, Balancing machine vibration and identification of oil-film bearing parameteres, Proceedings of the Engineering Mechanics 2006, Svratka, 2006, pp. 133-144.

[9] V. Zeman, J. Kellner, Mathematical modelling of bladed disk vibration. Proceedings of the 22nd Computational Mechanics, Nectiny, University of West Bohemia in Pilsen, 2006, pp. 713-720.